Localized fracture of repair material in patch repair systems

M. Kunieda, T. Kamada & K. Rokugo
Dept. of Civil Engineering, Gifu University, Gifu, Japan

J. E. Bolander
Dept. of Civil and Environ. Engrg., University of California, Davis,California, U.S.A.

ABSTRACT: This paper presents the effects of the properties of repair materials, such as crack distribution and toughness, on the fracture behavior of the repaired members. Both experimental and numerical results show that the geometry of the patch repair system can induce localized fracture within patch repair material itself. Though the ECC used as a patch repair material showed pseudo strain-hardening behavior, cracks did not uniformly distribute over the test area. The evaluation of crack distributions in a patch repair material should therefore be conducted with proper consideration of the geometry and boundary conditions at the crack site.

Keywords: patch repair system, ECC, zero-span elongation, crack distribution, RBSN

1 INTRODUCTION

Patch repair is one of the repair methods for deteriorated concrete structures. Performance requirements of the patch repair material include those related to strength, size stability, shieldability, durability, and bond property with the substrate concrete. In some cases, anti-spalling performance may be required for patch repair materials. Various kinds of short fibers, such as steel and polyvinyl alcohol (Vinylon) fibers, are currently included in patch repair materials to improve their toughness.

Various experiments have been conducted to determine the mechanical properties of members repaired by patch repair techniques. Engineered Cementitious Composites (ECC) that are strain-hardening type ductile fiber reinforced cementitious composites have been developed by Li (1993), and its applicability to patch repair (overlay systems) has also been investigated (Lim & Li 1997). The ECC in patch repair systems provides:

- narrow crack width that gives resistance to penetration of substances such as chloride ions, water and so forth, and
- tensile capacity and anti-spalling performance to repaired structures.

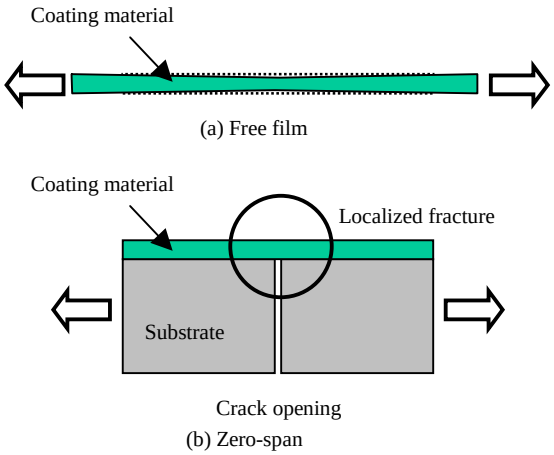

Figure 1. Elongation tests for surface coating materials

Usually, the performance of the ECC or other ductile materials is confirmed though tensile or bending tests with no restraint along the length of the test specimen.

In surface coating repair materials, such as epoxy and acrylic rubber, evaluation should not be performed only with free film elongation tests, as shown in Fig. 1. In a deteriorated concrete structure having cracks, the deformation of the members increases as cracks open wider. It means

that localized fracture occurs on the patch repair material near the cracks in substrate concrete. So, patch repair materials are required to follow the crack-opening motion under so-called zero-span elongation.

In this study, the effects of the properties of repair materials, such as crack distribution and toughness, on the fracture behavior of repaired members were investigated, both experimentally and numerically. It is clear that cracks in the substrate induce localized cracks within the repair material itself, and evaluating the toughness of patch repair materials under zero-span elongation is therefore important.

2 EXPERIMENTAL PROGRAM

2.1 *Outline of experiments*

2.1.1 *Production of substrate*

Table 1 gives the mix proportions of the substrate concrete. High-early-strength Portland cement with a density of 3.12 g/cm^3 was used at a water-cement ratio of 63%. Fine aggregate was river sand with a density of 2.59 g/cm^3. Coarse aggregate was crushed gravel with a density and maximum size of 2.61 g/cm^3 and 15mm, respectively. The specimens were demolded 2 days after concrete placing and cured in wet condition. The compressive strength and elastic modulus of the concrete at an age of 37 days (when the repaired specimens were subjected to loading) were 33 MPa and 25 GPa, respectively.

2.1.2 *Geometry of repaired specimens*

Specimens fabricated for the tests are indicated in Table 2. Three types of specimens were adopted to confirm the localized cracking behavior due to the conditions of the substrate concrete and the bond between the substrate and the ECC. As shown in Fig. 2(a), 100x100x800mm size beams were used for the specimens without an artificial crack. A patch repair material with a thickness of 30mm was placed on the substrate concrete. For specimens with an artificial crack, two beams (each having a size of 100x100x400mm) were carefully positioned with no clearance between them, as shown in Fig. 2(b). A patch repair material with a thickness of 30mm was placed over these beams. In addition, some specimens were made with a partially unbonded region above the artificial crack by applying a 50-mm wide gum tape prior to placing the repair material. This was done to investigate the effects of bond between substrate concrete and the patch repair material on the cracking behavior of the repair material itself (Fig. 2(c)).

In all cases, a water-jetting method was used to expose coarse aggregate and prepare the substrate concrete at an age of 15 days. The upper surfaces were all wetted immediately before placing of the patch repair material.

2.1.3 *Patch repair material*

The ECC was placed on the concrete as patch repair material at a concrete age of 16 days. This material exhibits pseudo strain-hardening and multiple cracking. Its mix proportions are given in Table 3. The water-cement ratio of the ECC was

Table 1. Mix proportions of substrate concrete

W/C (%)	Air (%)	Sl. (cm)	Unit content (kg/m^3)				
			Water	Cem.	Sand	Gravel	Ad.*
63	6.4	15	184	293	722	1035	11.7

*AE water reducing agent

Table 2. Repaired specimens

Artificial cracks	Surface treatment	Bond condition (the ECC&substrate)	Number of specimens
None	Water-jet	Fully bonded	2
Present		Fully bonded	2
		With unbonded region	2

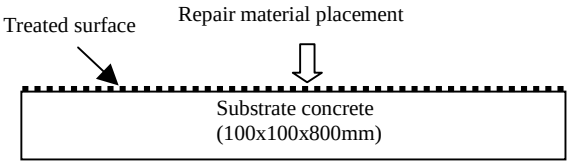

(a) Repaired specimens without artificial crack

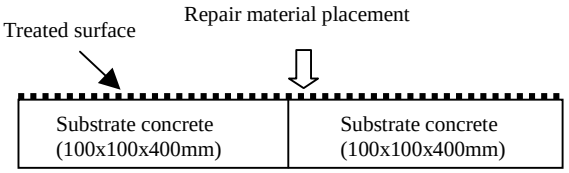

(b) Repaired specimens with artificial crack

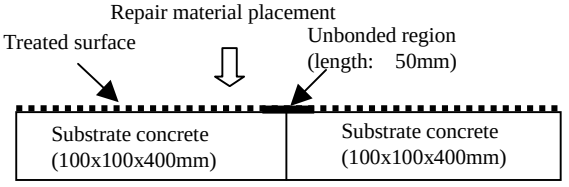

(c) Repaired specimens with unbonded area

Figure 2. Repaired specimens

30%. Polyethylene fibers ($12x10^{-6}$m in diameter and 12 mm in length) were included at a ratio of 1.5% by volume.

Uniaxial tensile tests were conducted on the ECC using dumbbell-shaped specimens to evaluate its tensile properties, as shown in Fig. 3. In consideration of the ECC thickness of 30mm for the repaired specimens, the cross sectional area in the center of dumbbell specimens was 30x30mm. Displacement was measured in three regions (Fig. 3) by using three pi-type displacement gauges with a range of 50mm (sensitivity: 1/2000 mm). Two specimens were tested.

The results of tensile tests on the dumbbell specimens are shown in Fig. 3. Here, the thick lines show the measurements by the gauge spanning the location where fracture ultimately localized. The first cracks occurred at approximately 4.5 MPa. Multiple cracking then followed, leading to rupture of the specimen after reaching the maximum stress of 5.2 MPa and a strain of approximately 2.5% over the guage length of 50 mm. However, the other measurements gave quite smaller strains due to localized fracture of the other part.

2.1.4 Loading method for repaired specimens

Four-point bending tests for the repaired specimens were carried out at a concrete age of 37 days (when the ECC age was 21 days). Figure 4 shows the specimens with the patched surface down on the tension side. For each specimen, pi-type displacement gauges (range: 50mm) were glued at four places on either side of the crack to measure the load-displacement relationship at each location indicated in the figure. The point of each place is 50mm apart from its counterpart across the crack plane.

2.2 *Test results of repaired specimens*

2.2.1 *Load-displacement curves*

Figure 5 shows the load-displacement curves obtained from the tests on the repaired specimens. Most specimens failed after reaching a displacement of 2 to 3mm, showing no marked effect of the artificial crack on the load-displacement curve. In the specimen with much larger displacement values, more than one crack occurred in the substrate concrete.

In this experiment, the unbonded region scarcely affected the shapes of the load-displacement curves of repaired specimens, except for the initial stiffness.

Table 3. Mix proportions of the ECC

Cem.*	Water	Sand**	Ad.1***	Ad.2****	Fiber(by vol. ratio)
1.0	0.30	0.31	0.030	0.00071	0.015

* High early strength Portland cement
** Silica sand
*** Superplasticizer
**** Viscosity agent (Cellulose)

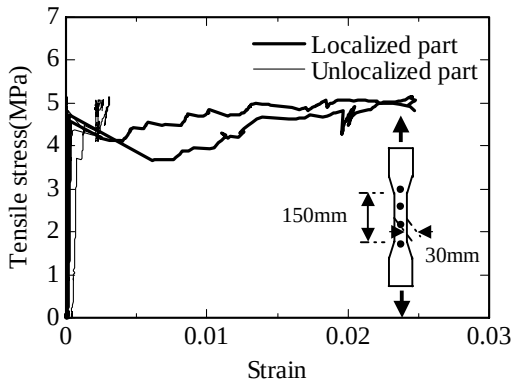

Figure 3. Tensile properties of the ECC

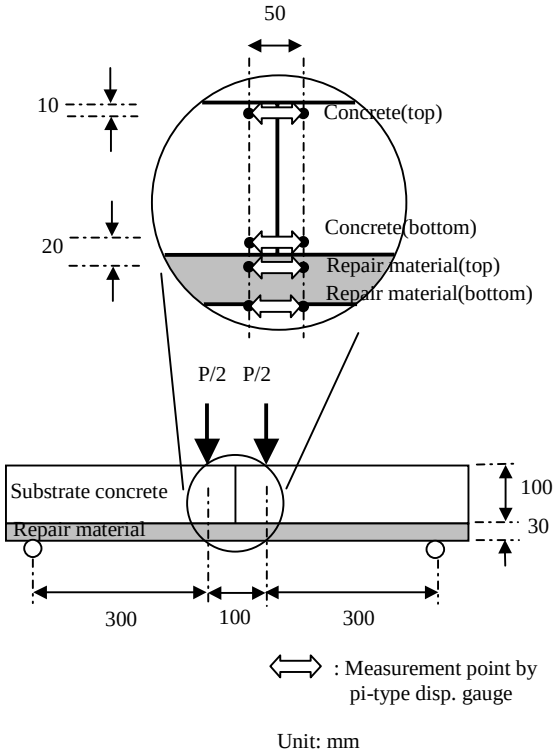

Figure 4. Geometry of repaired specimens

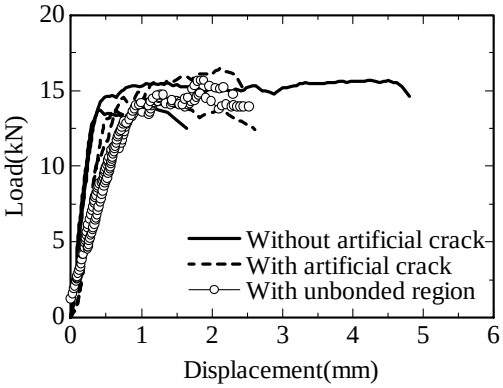

Figure 5. Load-displacement curves of repaired specimens

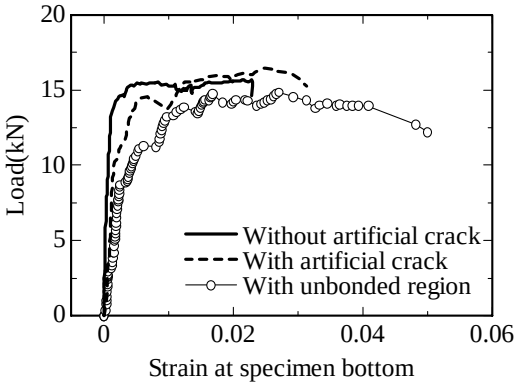

Figure 6. Typical load-strain curves of repaired specimens

2.2.2 *Load-strain curves for cracked site*

Figure 6 shows the load-strain curves measured at the specimen bottom. All the displacements were converted to strains with respect to the gauge length of 50mm.

Specimens with an artificial crack tended to show slightly lower initial stiffness. In such specimens, the strain was largest at approximately 3% on the bottom of the repaired specimens.

The strain of the specimens without an artificial crack tended to be lower than that of specimens with such a crack. This is because the measured part does not reach ultimate state (i.e. cracking occurred outside the range of the displacement gauges or some cracks occurred in the concrete in certain cases of specimens without an artificial crack.).

In the specimens with the unbonded region, the specimens fractured after generating a strain of approximately 5% on the bottom of the repaired specimens. The large strain can be attributed to the large area of the ECC that can contribute to deformation without being restrained by the substrate concrete.

2.2.3 *Cracking behavior*

Figures 7 and 8 show typical crack patterns on the repaired specimens. Diagonal cracks occurred within the ECC near the specimen center, and this set of cracks has an overall triangular shape, regardless of the presence/absence of an artificial crack. The length of the cracked part at the bottom was approximately 30 to 50mm along the beam axis. In specimens having an unbonded region, the length of the crack site on the bottom of the

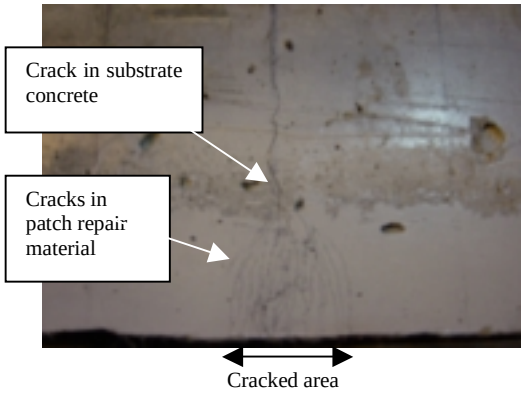

Figure 7. Crack pattern of repaired specimen (without artificial crack)

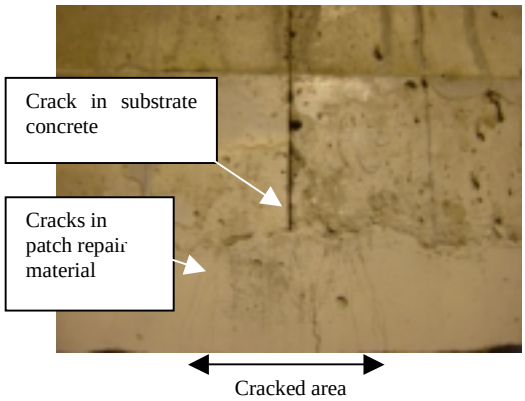

Figure 8. Crack pattern of repaired specimen (with artificial crack and un-bonded part)

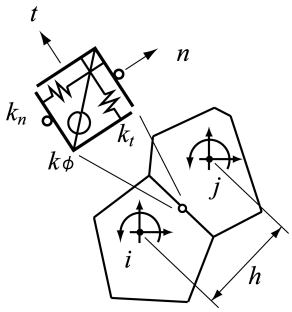

(a) Two-cell assembly

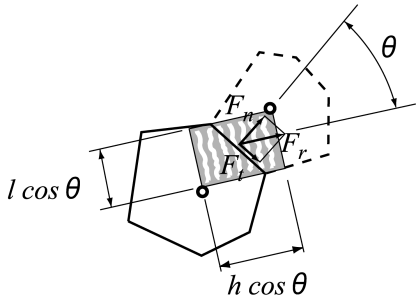

(b) Rotating crack band concept

Figure 9. RBSN model

ECC was longer than that of fully bonded specimens.

3 NUMERICAL PROCEDURES

3.1 *RBSN approach*

Rigid-Body-Spring Networks (RBSN) developed by Bolander and Saito (1998) were used to model the repaired specimens. In the RBSN approach, the material domain is discretized using a Voronoi diagram on a set of randomly distributed points. An element formed from two such points is shown in Fig. 9(a). Network degrees of freedom are defined at the Voronoi cell nuclei and system flexibility is lumped into zero-size spring sets that interconnect the cells. Each spring set consists of a normal, tangential and rotational springs. Spring stiffness is scaled in proportion to the distance between the cell nuclei, *h*, and the length of the common boundary segment, *l*.

Tensile fracture within the RBSN is represented using the crack band concept of Bažant and Oh (1983). For the tensile type loadings considered here, an alternative approach is used, which is a sort of rotating crack band model (Bolander et al. 2001). The crack band is assumed to form perpendicular to the resultant, *Fr*, of the forces in the normal and tangential springs, as shown in Fig. 9 (b).

The experimental procedures and results shown in Section 2 are used for comparison. The discretized model of the repaired specimen is shown in Fig. 10. The specimen configuration is

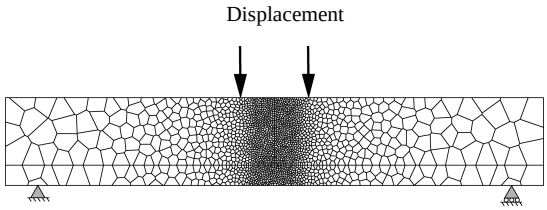

Figure 10. Modeled repaired specimen

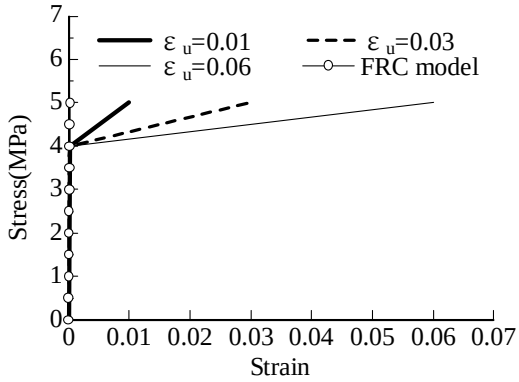

(a) Hardening behavior

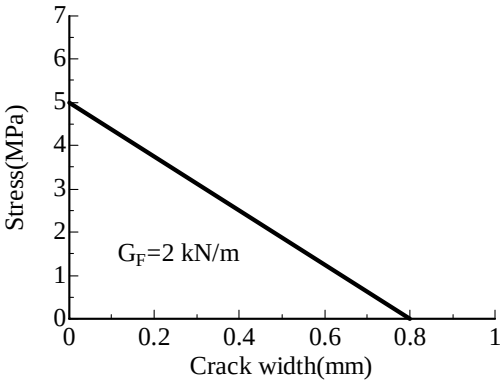

(b) Softening behavior (all cases)

Figure 11. Constitutive model for fracture

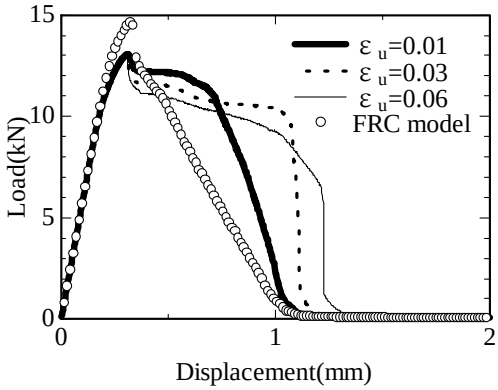

Figure 12. Load-displacement curves of the specimens without artificial crack

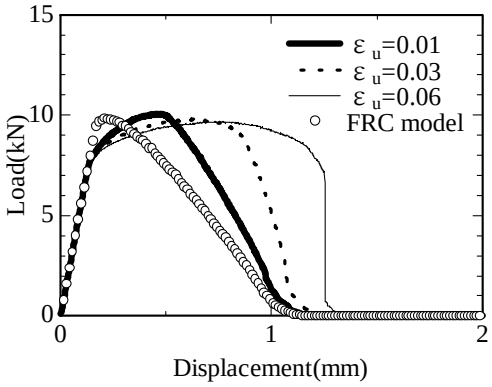

Figure 13. Load-displacement curves of the specimens with an artificial crack

modeled by the Voronoi diagram. The size of each Voronoi cell is gradually changed to reduce computational time. The distance between the cell nuclei, *h*, in the constant moment span is about 3 mm.

3.2 *Modeling of fracture*

3.2.1 *Substrate concrete*

Tensile strength and elastic modulus of the substrate were assumed to be 3.3MPa and 25GPa, respectively. After cracking, a bi-linear softening relation based on the 1/4 model of Rokugo et al. (1989) was used with G_F = 150N/m.

3.2.2 *Patch repair materials (ECC)*

Tensile strength and elastic modulus of the ECC were 5MPa and 22GPa, respectively. The strength and dissipated energy of each spring set are defined according to a stress-strain relation, such as that shown in Fig. 11. The stress-strain relation consists of two phases:

- a hardening region that exhibits multiple cracking up to maximum stress (Fig. 11(a)),
- a softening region due to localized cracking after maximum stress (Fig. 11(b)).

In the hardening region, three stress-strain relations were assumed. Initial crack occurs at the stress of $0.8F_t$ (i.e. 4.0MPa). In the softening region, the linear softening relation shown in Fig. 11(b) was used in all cases. The critical crack width, W_{cr}, is assumed to be 0.8mm, and this means that the fracture energy, G_F, is 2kN/m. For modeling of compression, the material is assumed to have elastic behavior.

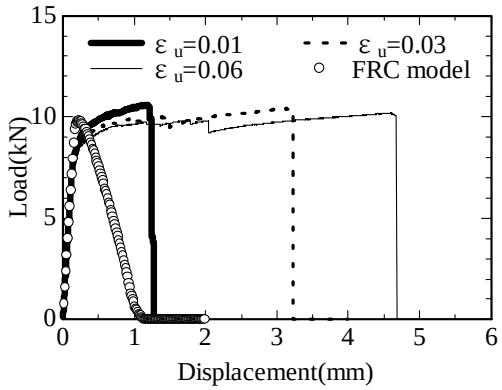

Figure 14. Load-displacement curves of the specimens with unbonded region

For comparison, a FRC model (that does not include strain-hardening) was also analyzed. It was based on a tensile strength of 5MPa and fracture energy of 2kN/m.

3.2.3 *Modeling of artificial cracks and unbonded region*

In the experiments, some specimens contained an artificial crack and/or an unbonded region. These features were modeled by allowing the springs to transfer only compressive stress, when appropriate.

3.3 *Analytical results*

3.3.1 *Load-displacement curves*

Figures 12 and 13 show the load-displacement curves of repaired specimens with the presence/absence of the artificial crack in the substrate concrete. The difference of maximum

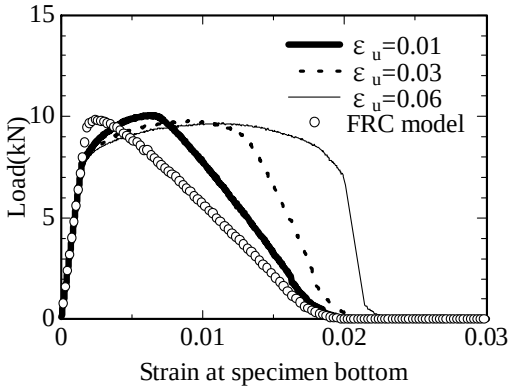

Figure 15. Load- strain curves of the specimens without unbonded region

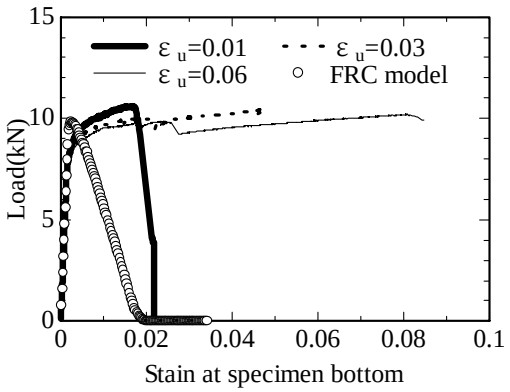

Figure 16. Load- strain curves of the specimens with unbonded region

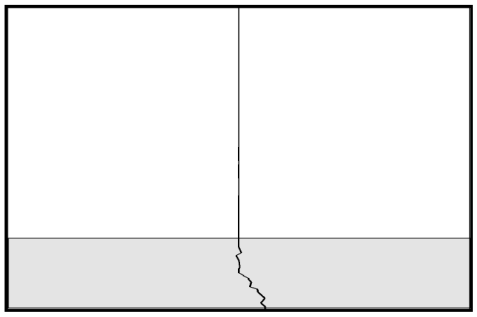

Figure 17. Crack pattern(ε_u=0.01, Disp.=0.5mm)

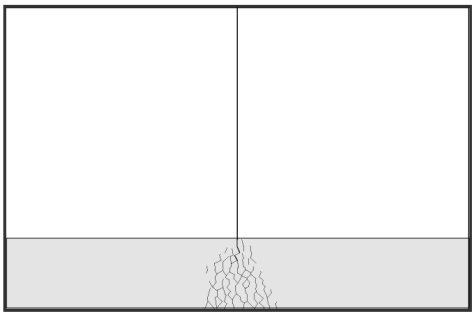

Figure 18. Crack pattern(ε_u=0.03, Disp.=0.8mm)

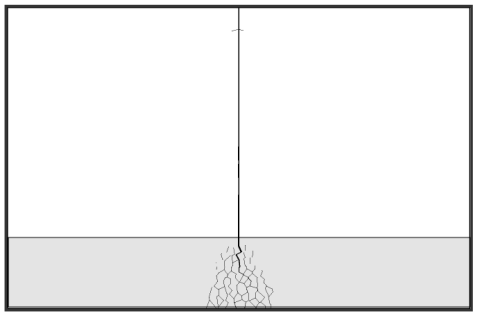

Figure 19. Crack pattern(ε_u=0.06, Disp.=1.2mm)

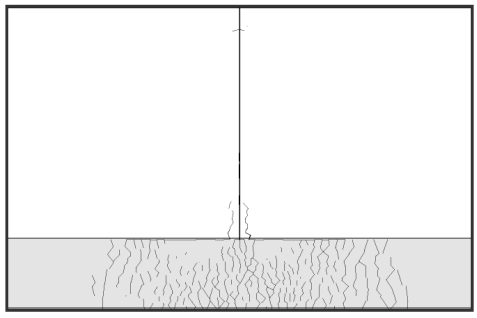

Figure 20. Crack pattern(unbonded region, ε_u=0.01, Disp.=1.2mm)

strain of patch repair material itself, which was an input value, did not affect the displacement up to where the load decreased suddenly. In addition, the effect of the artificial crack on the load-displacement curves is not significant, except for the peak load. The peak loads of the specimens without an artificial crack were higher than those with one, because of the ability to carry tensile stress in the substrate concrete.

The load-displacement curves of the specimens with an unbonded region are shown in Fig. 14. The displacement at the maximum load was strongly affected by the maximum strain in the constitutive models (input values). However, there is only a slight difference within the FRC model, even if an unbonded region is used, because the FRC model exhibits localized fracture in all cases.

The calculated strains at the bottom of the repaired specimens, within the gauge length of

50mm, are shown in Figs. 15 and 16. The calculated maximum strains in Fig. 15 were smaller than the maximum strains of the original stress-strain relations (input values). This is because the localized fracture within the patch repair material was constrained by the substrate concrete. However, the maximum strains obtained from the repaired specimen with an unbonded region were larger than those without one, in all cases. The geometry of the patch repair system can induce localized fracture in patch repair material itself.

3.3.2 *Crack distribution*

Crack patterns for each repaired specimen, just before the sudden drop in load, are shown in Figs. 17-20. Here, the portrayed cracks have a crack width larger than 0.01mm, calculated by integrating the crack strain over the crack band width.

In the case of maximum strain of 0.01, the cracks are not uniformly distributed within the patch repair material. The material having the maximum strain of 0.01 may provide large deformation capacity and many cracks in an ordinary tensile test. So, the cracking behavior in patch repair system was different from that in ordinary material tests with no constraint. It is important to evaluate the material properties under conditions that reflect the existing boundary conditions, such as zero-span elongation.

In the case of maximum strains of 0.03 and 0.06, there were a set of cracks with narrow crack width, and the overall shape of the cracked zone was triangular. However, the difference of crack patterns in each case (i.e. maximum strains of 0.03 and 0.06) was not clear due to localized fracture of the patch repair materials.

As shown in Fig. 19, the unbonded region exhibited uniformly distributed cracks within the patch repair material, which also agrees well with the experimental results.

4 CONCLUSIONS

The following conclusions were obtained from the study:

- The geometry of the patch repair system can induce localized fracture within patch repair material itself. Though the ECC used as a patch repair material showed pseudo strain-hardening behavior, cracks did not uniformly distribute over the test area. The evaluation of crack distributions in a patch repair material should therefore be conducted with due consideration of the boundary conditions at the crack site.
- In the experiments, an unbonded region between the concrete and the ECC did not affect the shape of load-displacement curves. Instead, it strongly affected the load-strain relationship based on pi-gauge measurements. This may be attributed to the fact that, in specimens with an unbonded region between concrete and ECC, a large area of the ECC could contribute to deformation without being restrained by the concrete. With an unbonded region, the length of the distributed crack zone on the specimen bottom was longer than without an unbonded region.
- The localized fracture in the repaired specimens was well simulated by the numerical model. From the analysis, the effect of the maximum strain in repair materials on crack distribution or load-displacement relations was not significant, in the case without an unbonded region. However, an unbonded region imparted both uniform crack distribution and higher ductility in the load-displacement curves of repaired specimens. In addition, the softening materials, such as ordinary short fiber reinforced materials, were not affected by the presence of an un-bonded region.

5 REFERENCES

Bažant, Z. P. & Oh, B. H., 1983, Crack band theory for fracture of concrete, Materials and Structures, RILEM, Vol. 16, pp.155-176

Bolander, J. & Saito, S., 1998, Fracture analysis using spring networks with random geometry, Engineering Fracture Mechanics, Vol. 61, No.5-6, pp.569-591

Bolander, J. E., Yip, M., Moriizumi, K. & Kunieda, M., 2001, Rigid-Body-Spring Network modeling of cement-based composites, Fracture Mechanics of Concrete Structures, A.A. BALKEMA PUBLISHERS, pp.773-780

Li, V. C., 1993, From micromechanics to structural engineering - the design of cementitious composites for civil engineering applications, Journal of Structural Mechanics and Earthquake Engineering, JSCE, Vol. 10, No. 2, pp.37-48

Lim, Y. M. & Li, V. C., 1997, Durable repair of aged infrastructures using trapping mechanism of engineered cementitious composites, Journal of Cement and Concrete Composites, Elsevier, Vol. 19, No. 4, pp.373-385

Rokugo, K., Iwasa, M., Suzuki, T. & Koyanagi W., 1989, Testing methods to determine tensile strain softening curves and fracture energy of concrete, Fracture Toughness and Fracture Energy, Balkema, Rotterdam, pp. 153-163